Trends and source apportionment of aerosols in Europe during 1980–2018

Yang Yang[1], Sijia Lou[2*], Hailong Wang[3], Pinya Wang[1], Hong Liao[1]

[1]Jiangsu Key Laboratory of Atmospheric Environment Monitoring and Pollution Control, Jiangsu Collaborative Innovation Center of Atmospheric Environment and Equipment Technology, School of Environmental Science and Engineering, Nanjing University of Information Science and Technology, Nanjing, Jiangsu, China

[2]School of Atmospheric Sciences, Nanjing University, Nanjing, Jiangsu, China

[3]Atmospheric Sciences and Global Change Division, Pacific Northwest National Laboratory, Richland, Washington, USA

*Correspondence to lousijia@nju.edu.cn

22   **Abstract**

23   Aerosols have significantly affected health, environment and climate in Europe.

24   Aerosol concentrations have been declining since 1980s in Europe, mainly owing to

25   the reduction of local aerosol and precursor emissions. Emissions from other source

26   regions of the world, which have been changing rapidly as well, may also perturb the

27   historical and future trends of aerosols and change their radiative impact in Europe.

28   This study examines trends of aerosols in Europe during 1980–2018 and quantify

29   contributions from sixteen source regions using the Community Atmosphere Model

30   version 5 with an Explicit Aerosol Source Tagging technique (CAM5-EAST). The

31   simulated near-surface total mass concentration of sulfate, black carbon and primary

32   organic carbon had a 62% decrease during 1980–2018, of which the majority was

33   contributed by reductions of local emissions in Europe and 8%-9% was induced by

34   the decrease in emissions from Russia-Belarus-Ukraine. With the decreases in the

35   fractional contribution of local emissions, aerosols transported from other source

36   regions are increasingly important to air quality in Europe. During 1980–2018, the

37   decrease in sulfate loading leads to a warming effect of 2.0 W m^{-2} in Europe, with

38   12% coming from changes in non-European sources, especially from North America

39   and Russia-Belarus-Ukraine. According to the Shared Socioeconomic Pathways

40   (SSP) scenarios, contributions to the sulfate radiative forcing over Europe from both

41   European local emissions and non-European emissions would decrease at a

42   comparable rate in the next three decades, suggesting that future changes in non-

43   European emissions are as important as European emissions in causing possible

44   regional climate change associated with aerosols in Europe.

45

46

47

1. Introduction

Aerosols are main air pollutants that contribute to excess morbidity and premature mortality through damaging cardiovascular and respiratory systems (Lelieveld et al., 2019). They also have adverse effects on atmospheric visibility for road and air traffic (Vautard et al., 2009). During the 1952 London Fog, high fatality associated with extremely high level of aerosols caused thousands of premature deaths (Bell and Davis, 2001), which resulted in a number of air quality legislations for reducing air pollution in Europe (Brimblecombe et al., 2006).

Besides the health and environment effects, aerosols can significantly impact regional and global climate through perturbing the Earth's radiation fluxes and influencing cloud microphysics (Boucher et al., 2013). Globally, anthropogenic aerosols exert a net cooling effect in the Earth system, which have dampened the warming driven by greenhouse gases since the pre-industrial era. Due to a strong surface albedo feedback over polar regions, per unit aerosol emission from western Europe was reported to have the greatest cooling effect than other major source regions of the globe (Persad and Caldeira, 2018), revealing the importance of understanding aerosol variations in Europe.

Significant reductions in near-surface aerosol concentrations and aerosol optical depth (AOD) have been observed in Europe during the last few decades from long-term station measurements and satellite retrievals (de Meij et al., 2012; Tørseth et al., 2012). The decrease in aerosols has been considered as a cause of the increase in surface solar radiation over Europe since the 1980s (Wild, 2009), as well as the

70   contributor of the eastern European warming (Vautard et al., 2009), Arctic

71   amplification (Acosta Navarro et al., 2016), and the increased atmospheric visibility

72   over Europe (Stjern et al., 2011) during the past three decades.

73   The decrease in aerosols over Europe was mainly attributed to the continuous

74   reductions in European local anthropogenic emissions of aerosols and precursor

75   gases since the 1980s (Smith et al., 2011), as a result of legislations for improving

76   air quality. In addition to local emissions, aerosol levels can also be affected by

77   aerosol transport at continental scales (Zhang et al., 2017; Yang et al., 2018a).

78   Aerosol emissions in major economic regions of the world have been changing

79   rapidly during the past few decades owing to economic development and

80   environmental measures. North America has started reducing emissions since the

81   1980s, and emissions in Russia also showed decreasing trends after the dissolution

82   of the Soviet Union (Smith et al., 2011). In the meantime, aerosol emissions from

83   East Asia and South Asia have largely increased due to economic growth, although

84   emissions in China have been undergoing a remarkable reduction in the most recent

85   years, as a result of strict air quality regulations (Streets et al., 2000; Li et al., 2017).

86   It is important to understand the relative roles of local emissions and regional

87   transport in affecting long-term variation of aerosols in Europe from both air quality

88   and climate perspectives.

89   Source apportionment is useful for quantifying contributions to aerosols from

90   specific source regions and/or sectors, which is beneficial to the emission control

91   strategies. The traditional method of examining the source-receptor relationship in

92   aerosol models is to zero out or perturb a certain percent of emissions from a given

93   source region or sector in parallel sensitivity simulations along with a baseline

94   simulation, which has been used in many studies to examine source contributions of

95   particulate matter (PM) in Europe from different sectors (e.g., Sartelet et al., 2012;

96   Tagaris et al., 2015; Aksoyoglu et al., 2016). Recently, source region contributions to

97   European CO and O_3 levels, as well as global and regional aerosol radiative forcing,

98   were examined under the Hemispheric Transport of Air Pollution model experiment

99   phase 2 (HTAP2) protocol, in which sensitivity simulations were conducted with

100   anthropogenic emissions from different source regions reduced by 20% (Jonson et

101   al., 2018). This method suffers a large computational cost for the excessive model

102   simulations when estimating contributions from a large number of sources, and

103   contributions from all sources do not sum up to 100% of the total concentration in the

104   default simulation (Koo et al., 2009; Wang et al., 2014).

105   The explicit aerosol tagging method, which simultaneously tracks contributions

106   from many different sources, is a useful tool for assessing source-receptor

107   relationship of aerosols. This method has previous been adopted in regional air

108   quality models such as CAMx (the Comprehensive Air quality Model with

109   Extensions) and CMAQ (the Community Multi-scale Air Quality model). Using

110   regional air quality models with aerosol tagging, contributions from different source

111   sectors and local/regional sources to European PM and its health impact were

112   studied (Brandt et al., 2013; Skyllakou et al., 2014; Karamchandani et al., 2017).

113   However, due to the limitation in domain size of regional air quality models,

114   contributions of intercontinental transport from sources outside the domain are

115   difficult to be accounted.

116   Anthropogenic emissions of aerosols and their precursor gases from different

117   economic regions of the world have changed substantially during the past few

118   decades. Very few studies have examined the source apportionment of aerosols in

119   Europe from sources all over the changing world. In this study, source attributions of

120   concentrations, column burden, optical depth of aerosols in four major areas of

121   Europe from sixteen source regions of the globe over 1980–2018 are quantified,

122   which is facilitated by the explicit aerosol source tagging technique that were recently

123   implemented in a global aerosol-climate model (CAM5-EAST). This technique has

124   lately been used to examine source attribution of aerosol trends in China and U.S.

125   during 1980–2014 (Yang et al., 2018a,b). The source apportionment analysis is

126   extended to year 2018 using the Shared Socioeconomic Pathways (SSPs) scenario,

127   with a focus on Europe here.

128   The CAM5-EAST model, along with the aerosol source tagging technique, and

129   aerosol emissions are described in Sect. 2. Section 3 evaluates the model

130   performance in simulating aerosols in Europe. Section 4 show the analysis of

131   source-receptor relationships of aerosols in Europe in climatological mean. Source

132   contributions to long-term variations of European aerosols and their direct radiative

133   forcing (DRF) during 1980–2018, as well as future forcing prediction, are provided in

134   Sect. 5. Section 6 summarizes these results and conclusions.

135   **2. Methods**

2.1 Model Description and Experimental Setup

136

137   The global aerosol-climate model CAM5 (Community Atmosphere Model version

138   5), which was developed as the atmospheric component of CESM (the Community

139   Earth System Model, Hurrell et al., 2013), is applied to simulate aerosols at a spatial

140   resolution of 1.9° latitude × 2.5° longitude and 30 vertical layers from the surface to

141   3.6 hPa. Aerosol species, including sulfate, black carbon (BC), primary organic

142   aerosol (POA), second organic aerosol (SOA), mineral dust and sea salt, can be

143   simulated in a modal aerosol module of CAM5. The three-mode aerosol module

144   (MAM3) configuration is chosen with the consideration of the computational

145   efficiency of long-term simulation. Details of the MAM3 aerosol representation in

146   CAM5 are described in Liu et al. (2012). On top of the default CAM5, some aerosol-

147   related scheme modifications are utilized to improve the model performance in the

148   aerosol convective transport and wet deposition (Wang et al., 2013).

149   A 40-year (1979–2018) historical AMIP-type (Atmospheric Model

150   Intercomparison Project) simulation has been performed, following CMIP6 (the

151   Coupled Model Intercomparison Project Phase 6) configurations and forcing

152   conditions. Time-varying sea surface temperatures, sea ice concentrations, solar

153   insolation, greenhouse gas concentrations and aerosol emissions are prescribed in

154   the simulation. To better reproduce large-scale circulation patterns for aerosol

155   transport in the model, wind fields are nudged to the MERRA-2 (Modern Era

156   Retrospective-Analysis for Research and Applications Version 2) reanalysis (Ronald

157   Gelaro et al., 2017).

158   Aerosol DRF is defined in this study as the difference in clear-sky radiative fluxes

159   at the top of the atmosphere between two diagnostic calculations in the radiative

160   transfer scheme with and without specific aerosol species accounted, respectively.

161   Historical variation of sulfate DRF due to anthropogenic emissions from Europe and

162   outside Europe are quantified in this study. Rather than sulfate, DRF of other aerosol

163   species is not calculated in this study due to the computational limitation considering

164   multiple source regions. However, because sulfate dominates the decrease in total

165   combustion AOD in Europe shown below, the sulfate DRF is calculated to roughly

166   represent the DRF caused by the total combustion AOD change. Future DRF of

167   sulfate aerosol over Europe is also estimated through scaling historical mean (1980–

168   2018) sulfate DRF by the ratio of SSPs future SO_2 emissions to historical emissions

169   assuming a linear response of DRF to AOD and regional emissions. This DRF

170   prediction method has been used to estimate the East Asian contribution to sulfate

171   DRF in U.S. in 2030s (Yang et al., 2018a).

172   **2.2 Aerosol Source Tagging Technique**

173   The Explicit Aerosol Source Tagging (EAST) technique, which was recently

174   implemented in CAM5 (Wang et al., 2014; Yang et al., 2017a, b), is used to examine

175   the long-term source apportionment of aerosols in Europe. Unlike the traditional

176   back-trajectory and emission perturbation methods, EAST has the identical physical,

177   chemical and dynamical processes considered independently for aerosol species

178   (defined as new tracers) emitted from each of the tagged source region and/or sector

179   in the simulation. Sulfate, BC, POA and SOA from pre-defined sources can be

180 explicitly tracked, from emission to deposition, in one CAM5-EAST simulation. Due

181 to the computational constraint and potentially large model bias from the simplified

182 SOA treatment (Yang et al., 2018a; Lou et al., 2019), we focus on sulfate, BC and

183 POA in this study but quantify the potential impact of SOA on the aerosol variation.

184   The global aerosol and precursor emissions are decomposed into sixteen source

185 regions defined in the HTAP2 protocol, including Europe (EUR), North America

186 (NAM), Central America (CAM), South America (SAM), North Africa (NAF), South

187 Africa (SAF), the Middle East (MDE), Southeast Asia (SEA), Central Asia (CAS),

188 South Asia (SAS), East Asia (EAS), Russia-Belarus-Ukraine (RBU), Pacific-

189 Australia-New Zealand (PAN), the Arctic (ARC), Antarctic (ANT), and Non-

190 Arctic/Antarctic Ocean (OCN) (Figure 1). Note that sources from marine and volcanic

191 eruptions are included in OCN. The focused receptor region in this study is Europe,

192 which is further divided into Northwestern Europe (NWE or NW Europe),

193 Southwestern Europe (SWE or SW Europe), Eastern Europe (EAE or E. Europe)

194 and Greece-Turkey-Cyprus (GTC) based on the finer source region selection in

195 HTAP2.

196 **2.3 Aerosol and Precursor Emissions**

197   Following the CMIP6-AMIP protocol, historical anthropogenic (Hoesly et al.,

198 2018) and biomass burning (van Marle et al., 2017) emissions of aerosol and

199 precursor gases are used over 1979–2014. For the remaining four years (2015–

200 2018), emissions are interpolated from the SSP2-4.5 forcing scenario, in which

201 aerosol pathways are not as extreme as other SSPs and have been used in many

202   model intercomparison projects for CMIP6 (O'Neill et al., 2016). Figure S1 shows the

203   spatial distribution and time series of anthropogenic emissions of SO_2 (precursor gas

204   of sulfate aerosol), BC and POA from Europe over 1980–2018. High emissions are

205   located over E. Europe and NW Europe, from which the emissions of SO_2, BC and

206   POA were reduced by 84–93%, 43–62% and 28–36%, respectively, in 2014–2018

207   relative to 1980–1984. Although SW Europe had a relatively low total amount of

208   emissions compared to E. Europe and NW Europe, it had significant reductions in

209   SO_2 and BC emissions, 91% and 55%, respectively. Over GTC region, SO_2 and BC

210   emissions were increased by 49% and 48%, respectively. Considering the sub-

211   regions as a whole, SO_2, BC and POA emissions from Europe have decreased by

212   12.57 Tg yr^{-1} (83%), 0.22 Tg yr^{-1} (46%) and 0.30 Tg yr^{-1} (24%) in 2014–2018

213   compared to 1980–1984 (Table 1). Historical changes in emissions from other

214   source regions can be found in Hoesly et al. (2018) and Yang et al. (2018b).

215   **3 Model Evaluation**

216   EMEP (European Monitoring and Evaluation Programme, http://www.emep.int)

217   networks provide daily near-surface aerosol concentrations in Europe. The annual

218   mean of daily observations is used to evaluate the model performance in this study.

219   Compared to the observational data from EMEP networks during 2010–2014, CAM5-

220   EAST can well reproduce the spatial distribution and magnitude of aerosol

221   components with normalized mean biases (NMB) of -14%~-23% and correlation

222   coefficients (R) in a range of 0.43~0.62 for sulfate, BC and organic carbon (OC,

223   derived from POA and SOA from the model results) (Figures 2).

224   Figure 3 shows the time series of annual mean near-surface sulfate, BC, and OC

225   concentrations averaged over EMEP sites in Europe and the corresponding model

226   values during 1993–2018. Variations in near-surface sulfate concentrations are

227   consistent between the model and observations, with R values higher than 0.9. The

228   observed variations of BC and OC concentrations in Europe are represented in the

229   simulation, with R values of 0.52 and 0.65, respectively. However, the observed high

230   values of BC and OC concentrations are not captured by the model, probably

231   because very few data were available before 2010 and, therefore, any difference

232   between model and observation cannot be smoothed out through the spatial

233   average. This is also indicated by the large spatial variation of BC and OC

234   concentrations before 2010. Nevertheless, the modeled concentrations are still

235   within the range of observations. Note that the number of sites used for the spatial

236   average in Figure 3 is different from year to year and thus the variation or trend here

237   does not represent that over a sub-region or the entire Europe.

238   The modeled AOD is evaluated against the AERONET (Aerosol Robotic

239   Network, https://aeronet.gsfc.nasa.gov) data in Figure 8. Both the modeled and

240   observed AOD show decreasing trends during 2001–2018. The model

241   underestimates AOD in all four sub-regions of Europe probably due to the lack of

242   nitrate aerosol. The variations of AOD in Western Europe (combined NW and SW

243   Europe) are well predicted with R values of about 0.75, but the model barely

244   reproduces the AOD variations in E. Europe and the GTC region (R<0.5). The

245   difference of the interannual variation in AOD between the model simulation and

246   observation can be caused by many factors such as aerosol emissions, aerosol

247   parameterizations in model, aerosol mixing state, inaccurate meteorological fields

248   from reanalysis data, and biases in measurements. However, identifying the

249   contribution of each factor to the difference is beyond the scope of this paper.

250   **4. Source Apportionment of Aerosols in Europe**

251   Based on the tagging technique in CAM5-EAST, near-surface concentrations of

252   total sulfate-BC-POA can be attributed to emissions within and outside Europe, as

253   shown in Figures 4a and 4b, and the relative contributions in percentage are given in

254   Figures 4c and 4d. Averaged over 2010–2018, due to the relatively high local

255   emissions, annual mean sulfate-BC-POA concentrations contributed by European

256   emissions show peak values of 4 µg m^{-3} in E. Europe. The slight increase in SO$_2$

257   emission from the GTC region (Figure S1), which is opposite to the decreases in the

258   other three sub-regions of Europe, also leads to high concentrations in GTC, with 2–

259   4 µg m^{-3} contributed by European emissions. Due to the atmospheric transport from

260   surrounding regions including North Africa, the Middle East and Russia-Belarus-

261   Ukraine, non-European emissions account for 0.5–1 µg m^{-3} over SW Europe, E.

262   Europe and GTC area. Overall, European local emissions are the dominant sources

263   of sulfate-BC-POA near-surface concentrations in Europe with contributions larger

264   than 80% (60%) in central areas (most of Europe). Non-European emissions are

265   responsible for 30–50% of the near-surface concentrations near the coastal areas

266   and boundaries of the Europe that are easily influenced by aerosol regional

267   transport.

268   Figure 5 illustrates the source contributions in percentage of emissions from

269   different regions of the globe to near-surface aerosol concentrations and column

270   burdens over the four sub-regions of Europe averaged over 2010–2018. Different

271   aerosols have fairly different local/remote source attributions depending on the local

272   to remote emission ratio and transport efficiency. European emissions explain 54%–

273   68% of near-surface sulfate concentrations over the four sub-regions of Europe, with

274   the largest local contribution in E. Europe due to the relatively high emission rate.

275   The emissions from Europe dominate BC and POA concentrations in Europe with

276   contributions in the range of 78%–95% and 58%–78%, respectively. The impact of

277   local emissions on near-surface sulfate concentration is smaller than BC and POA.

278   This is partially due to the less efficient gas scavenging than particles and the

279   additional SO_2-to-sulfate conversion process that increases the atmospheric

280   residence time of sulfur. On the other hand, the higher initial injection height of SO_2

281   emissions from some sources (e.g., industrial sector and power plants) facilitates the

282   lifting of SO_2 and sulfate aerosol into the free atmosphere and, therefore, favors the

283   long-range transport (Yang et al., 2019). The efficient reduction in local SO_2

284   emissions in Europe also caused the lower influences of local emissions on sulfate

285   concentrations in recent years.

286   Anthropogenic emissions over oceans (e.g., international shipping) and natural

287   emissions of oceanic dimethyl sulfide (DMS) and volcanic activities together account

288   for 16%–28% of near-surface sulfate concentrations in the four sub-regions of

289   Europe. About 10% of sulfate and 5%–10% of BC and POA in E. Europe and GTC

290   come from Russia-Belarus-Ukraine emissions. North Africa contributes to 7% of

291   sulfate, 17% of BC and 24% of POA over SW Europe. The contributions of

292   emissions, from the Middle East, to aerosol concentrations in GTC are between 5%

293   and 10%.

294   The transboundary and intercontinental transport of aerosols occur most

295   frequently in the free troposphere rather than near the surface, as horizonal transport

296   pathways at the surface and 500 hPa are indicated on the spatial distribution map of

297   the relative contributions shown in Figures S2 and S3. This also leads to larger

298   relative contributions from non-European sources to aerosol column burdens than to

299   the near-surface concentrations (Figure 5). The European emissions only contribute

300   32%–47% of column burden of sulfate, 57%–75% of BC and 51%–71% of POA over

301   the four sub-regions of Europe. Over NW Europe and SW Europe, about 10%–15%

302   of the sulfate burden is from East Asia and Russia-Belarus-Ukraine, respectively.

303   Sources in North Africa are responsible for 27% and 14% of BC and 19% and 11%

304   of POA burden over SW Europe and GTC, respectively. Emissions from North

305   America account for 15% and 10% POA burden over NW Europe and SW Europe,

306   respectively. Emissions from Russia-Belarus-Ukraine explain 12% and 19% of POA

307   burden over E. Europe and GTC, respectively. Since near-surface aerosol

308   concentrations directly affect air quality and column burden is more relevant to

309   radiative impact, the differences of relative contributions between near-surface

310   concentrations and column burden highlight the possible roles of non-local emissions

311   in either air quality or energy balance over Europe.

312   Source contributions to aerosols in Europe vary with season due to the

313   seasonality of emissions and meteorology. In general, local sources have the largest

314   contributions to both near-surface concentration and column burden of European

315   aerosols in winter and smallest contributions in summer averaged over 2010–2018

316   (outer rings in Figure 6). With the contributions normalized by the ratio of seasonal

317   anthropogenic emission to annual mean for each source, the impact of emission

318   seasonal variation on the source contributions can be removed (inner rings in Figure

319   6) (Yang et al., 2019). Without the influence of emission seasonality, local source

320   contributions decrease in winter and increase in summer, indicating that it was the

321   higher local anthropogenic emissions that result in the larger local source

322   contributions to wintertime aerosols in Europe relative to other seasons. Sulfur

323   sources over oceans account for one fourth to one third of European sulfate

324   concentration and burden in spring likely due to the strong westerlies in this season

325   that transport aerosols from the North Atlantic Ocean to the Europe. Source

326   contributions from Russia-Belarus-Ukraine and North America to BC and POA in

327   Europe show strong seasonal variabilities, which can be explained by the changes in

328   biomass burning emissions considering its large seasonal variability.

329 **5. Source Apportionment of Long-term Trends**

330   Total sulfate-BC-POA concentrations decreased during 1980–2018 over all of

331   the four sub-regions of Europe (Figure 7), since that near-surface aerosol

332   concentrations in Europe are dominated by its local emissions and the European

333   anthropogenic emissions have significantly decreased during this time period.

334   Averaged over the entire Europe, near-surface concentrations of sulfate, BC and

335   POA decreased by 70%, 43% and 23%, respectively, between 1980–1984 and

336   2014–2018, which is consistent with the decreases in local emissions (Table 1). The

337   total sulfate-BC-POA concentrations decreased by 62%. With SOA included, this

338   value does not have a substantial change (from 62% to 59%) and the decreasing

339   trends in the four sub-regions of the Europe are not largely affected either. The

340   column burden of sulfate, BC, POA and the sum of these three decreased by 60%,

341   28%, 4% and 55%, respectively, which is less than the decrease in corresponding

342   near-surface concentration. It is because non-local emissions have larger influences

343   at high altitudes than at the surface, which partly dampened the contribution of near-

344   surface aerosol decrease (induced by reductions in location emissions) to the

345   column integration.

346   The decrease in European local emissions explains 93% of the reduced

347   concentration and 91% of the reduced burden in Europe between the first and last

348   five-year period of 1980–2018, while 8%–9% is contributed by the reduction in

349   emissions from Russia-Belarus-Ukraine (Table 2). The decrease in emissions from

350   North America also explains 10% of the reduced column burden of sulfate-BC-POA

351   in Europe from 1980–1984 to 2014–2018. Along with the decreases in local emission

352   contributions to near-surface sulfate-BC-POA concentrations in Europe, the fraction

353   of non-European emission contributions increased from 10%–30% to 30%–50%

354   during 1980–2018 (Figure 7), indicating that aerosols from foreign emissions through

355   long-range transport have become increasingly important to air quality in Europe.

356 Regulations for further improvement of air quality in Europe in the near future need

357 to take changes in non-European emissions into account.

358   Similar to the declining trend in column burden, simulated total AOD also

359 decreased from 0.12–0.16 to 0.06–0.08 in NW Europe and SW Europe and from

360 0.19–0.21 to 0.09–0.13 in E. Europe and GTC region during the past four decades

361 (Figure 8). Sulfate AOD accounts for the largest portion of total combustion AOD

362 (sum of sulfate, BC, POA and SOA) over the four sub-regions of Europe. The

363 combustion AOD has decreased by 0.065 from 1980–1984 to 2014–2018 (Table 1),

364 with 0.059 (91%) contributed by the decrease in sulfate AOD. Therefore, we focus

365 on sulfate aerosol when examining the decadal changes in AOD and DRF in Europe

366 below.

367   The decreased sulfate AOD can also be decomposed into different contributions

368 from individual source regions in CAM5-EAST. European local emissions contribute

369 to 89% of the decrease, followed by 9% and 7% attributed to changes in emissions

370 from Russia-Belarus-Ukraine and North America, respectively, with the residual

371 offset by other source regions (Table 2). Over the last four decades, model simulated

372 sulfate AOD decreased at a rate of 0.017, 0.017, 0.026 and 0.012 decade^{-1},

373 respectively, over NW Europe, SW Europe, E. Europe and GTC. Decreases in

374 European local SO_2 emissions result in 78% of the sulfate AOD decreases over GTC

375 and about 90% over the other three sub-regions (Figure 9). For the remote sources,

376 emission changes in North America explain 5%–10% of the European sulfate AOD

377 decrease, while Russia-Belarus-Ukraine sources contribute 29% of the sulfate AOD

378   decrease over GTC and 6%–8% over NW Europe and E. Europe, indicating a

379   possible warming enhancement effect of changes in emissions from North America

380   and Russia-Belarus-Ukraine.

381   Averaged over 1980–2018, sulfate imposed a cooling effect over Europe with the

382   maximum negative DRF at the top of the atmosphere (TOA) exceeding –3 W m^{-2} in

383   E. Europe (Figure 10). Compared to 1980–1984, the magnitude of sulfate DRF

384   decreased in 2014–2018, leading to a 1–3 W m^{-2} warming mainly in E. Europe. The

385   warming effect mostly came from local SO_2 emission reduction, while non-European

386   emission changes only contributed less than 0.4 W m^{-2} over most regions of the

387   Europe. Considering Europe as a whole, the decrease in sulfate DRF caused a

388   warming effect of 2.0 W m^{-2}, with 88% and 12% coming from reductions European

389   local emissions and changes in non-European emissions, respectively (Tables 1 and

390   2).

391   Future changes in sulfate DRF associated with European and non-European

392   emissions based on eight SSP scenarios are also estimated and shown in Figure 11

393   and Figure S4 gives the estimate for each SSP scenario. Sulfate DRF contributed by

394   both European and non-European emissions would decrease in the near future but

395   has large variabilities between different SSPs. The sulfate DRF (cooling) over

396   Europe contributed from European local emissions shows a decrease from -0.48 W

397   m^{-2} in year 2015 to -0.18 (-0.08 ~ -0.33) W m^{-2} in year 2030 and -0.14 (-0.05 ~ -0.29)

398   W m^{-2} in year 2050. Unlike their contributions to the historical (1980–2018) change,

399   non-European emissions have an increasingly significant impact on the future sulfate

400 DRF changes in Europe. The contributions of non-European emissions decrease

401 from -0.68 W m^{-2} in year 2015 to -0.39 (-0.13 ~ -0.64) W m^{-2} in year 2030 and -0.26

402 (-0.08 ~ -0.63) W m^{-2} in year 2050, with the changes in a magnitude similar to that of

403 European local emissions. It suggests that future changes in non-European

404 emissions are as important as European emissions to radiative balance and

405 associated regional climate change in Europe.

406 **6. Conclusions**

407 Using a global aerosol-climate model with an explicit aerosol source tagging

408 technique (CAM5-EAST), we examine the long-term trends and source

409 apportionment of aerosols in Europe over 1980–2018 from sixteen source regions

410 covering the globe in this study. CAM5-EAST can well capture the spatial distribution

411 and temporal variation of aerosol species in Europe during this time period.

412 Averaged over 2010–2018, European emissions account for 54%–68%, 78%–

413 95% and 58%–78% of near-surface sulfate, BC, and POA concentrations over

414 Europe, respectively. Russia-Belarus-Ukraine emissions explain 10% of sulfate in E.

415 Europe and GTC. North Africa contributes to 17% of BC and 24% of POA over SW

416 Europe. Anthropogenic emissions over oceans (e.g., from international shipping) and

417 natural emissions from marine and volcanic activities together account for 16%–28%

418 of sulfate near-surface concentrations in Europe. European emissions only account

419 for 32%–47%, 57%–75% and 51%–71% of column burden of sulfate, BC and POA,

420 respectively, in Europe, with the rest contributed by emissions from East Asia,

421 Russia-Belarus-Ukraine, North Africa and North America. Source contributions of

422   aerosols in Europe vary with seasons driven by the seasonality of emissions and

423   meteorology.

424   Compared to 1980–1984, simulated total sulfate-BC-POA near-surface

425   concentration and column burden over 2014–2018 had a decrease of 62% and 55%,

426   respectively, the majority of which was contributed by reductions in European local

427   emissions. The decrease in emissions from Russia-Belarus-Ukraine contributed 8%–

428   9% of the near-surface concentration decrease, while the decrease in emissions

429   from North America accounted for 10% of the reduced column burden. With the large

430   decrease in local emission contribution, aerosols from foreign sources became

431   increasingly important to air quality in Europe. The decrease in sulfate led to a 2.0 W

432   m^{-2} warming in Europe, with 12% coming from changes in non-European emissions,

433   especially in North America and Russia-Belarus-Ukraine. Based on the SSP

434   scenarios and the assumed relationship between DRF and emissions, we estimated

435   that sulfate DRF over Europe contributed from European emissions and non-

436   European emissions would decrease at a comparable rate in the near future. This

437   suggests that future changes in non-European emissions are as important as

438   European emissions in affecting regional climate change associated with aerosols in

439   Europe. It should also be noted that the model currently does not have the ability to

440   simulate nitrate and ammonium aerosols and, therefore, the conclusions may not

441   hold with all aerosols.

442

443

444   *Data availability.*

445   The default CAM5 model is publicly available at

446   http://www.cesm.ucar.edu/models/cesm1.2/ (last access: 16 August 2019). Our

447   CAM5-EAST model code and results can be made available through the National

448   Energy Research Scientific Computing Center (NERSC) servers upon request.

449

450   *Competing interests.*

451   The authors declare that they have no conflict of interest.

452

453   *Author contribution*.

454   YY, SL, and HW designed the research; YY performed the model simulations; YY,

455   and SL analyzed the data. All the authors discussed the results and wrote the paper.

456

457   *Acknowledgments.*

458   This research was support by the National Natural Science Foundation of China

459   under grant 41975159, the U.S. Department of Energy (DOE), Office of Science,

460   Biological and Environmental Research as part of the Earth and Environmental

461   System Modeling program, Jiangsu Specially Appointed Professor Project, and the

462   Startup Fund for Talent at NUIST under Grant 2019r047. The Pacific Northwest

463   National Laboratory is operated for DOE by Battelle Memorial Institute under

464   contract DE-AC05-76RLO1830. The National Energy Research Scientific Computing

465   Center (NERSC) provided computational support.

References

Acosta Navarro, J. C., Varma, V., Riipinen, I., Seland, Ø., Kirkevåg, A., Struthers, Iversen, H., T., Hansson, H.-C., and Ekman, A. M. L.: Amplification of Arctic warming by past air pollution reductions in Europe, Nat. Geosci., 9, 277–281, https://doi.org/10.1038/ngeo2673, 2016.

Aksoyoglu, S., Baltensperger, U., and Prévôt, A. S. H.: Contribution of ship emissions to the concentration and deposition of air pollutants in Europe, Atmos. Chem. Phys., 16, 1895–1906, doi:10.5194/acp-16-1895-2016, 2016.

Bell, M. L., and Davis, D. L.: Reassessment of the Lethal London Fog of 1952: Novel Indicators of Acute and Chronic Consequences of Acute Exposure to Air Pollution, Environ. Health Perspect., 109, 389−394, https://doi.org/10.1289/ehp.01109s3389, 2001.

Boucher, O., Randall, D., Artaxo, P., Bretherton, C., Feingold, G., Forster, P., Kerminen, V. M., Kondo, Y., Liao, H., Lohmann, U., Rasch, P., Satheesh, S. K., Sherwood, S., Stevens, B., and Zhang, X. Y.: Clouds and Aerosols, in: Climate Change 2013: The Physical Science Basis, Contribution of Working Group I to the Fifth Assessment Report of the Intergovernmental Panel on Climate Change, edited by: Stocker, T. F., Qin, D., Plattner, G.- K., Tignor, M., Allen, S. K., Boschung, J., Nauels, A., Xia, Y., Bex, V., Midgley, P. M. Cambridge University Press, Cambridge, United Kingdom and New York, NY, USA, 571–658, 2013.

Brandt, J., Silver, J. D., Christensen, J. H., Andersen, M. S., Bønløkke, J. H., Sigsgaard, T., Geels, C., Gross, A., Hansen, A. B., Hansen, K. M., Hedegaard, G. B., Kaas, E., and Frohn, L. M.: Contribution from the ten major emission sectors in Europe and Denmark to the health-cost externalities of air pollution using the EVA model system – an integrated modelling approach, Atmos. Chem. Phys., 13, 7725–7746, https://doi.org/10.5194/acp-13-7725-2013, 2013.

Brimblecombe, P.: The Clean Air Act after 50 Years, Weather, 61, 311−314, https://doi.org/10.1256/wea.127.06, 2006.

de Meij, A., Pozzer, A., and Lelieveld, J.: Trend analysis in aerosol optical depths and pollutant emission estimates between 2000 and 2009, Atmos. Environ., 51, 75–85, https://doi.org/10.1016/j.atmosenv.2012.01.059, 2012.

Gelaro, R., McCarty, W., Suárez, M. J., Todling, R., Molod, A., Takacs, L., Randles, C. A., Darmenov, A., Bosilovich, M. G., Reichle, R., Wargan, K., Coy, L., Cullather, R., Draper, C., Akella, S., Buchard, V., Conaty, A., da Silva, A. M., Gu, W., Kim, G.-K., Koster, R., Lucchesi, R., Merkova, D., Nielsen, J. E., Partyka, G., Pawson, S., Putman, W., Rienecker, M., Schubert, S. D., Sienkiewicz, M., and

Zhao, B.: The Modern-Era Retrospective Analysis for Research and Applications, Version 2 (MERRA-2), J. Climate, 30, 5419–5454, https://doi.org/10.1175/JCLI-D-16-0758.1, 2017.

Hoesly, R. M., Smith, S. J., Feng, L., Klimont, Z., Janssens-Maenhout, G., Pitkanen, T., Seibert, J. J., Vu, L., Andres, R. J., Bolt, R. M., Bond, T. C., Dawidowski, L., Kholod, N., Kurokawa, J.-I., Li, M., Liu, L., Lu, Z., Moura, M. C. P., O'Rourke, P. R., and Zhang, Q.: Historical (1750–2014) anthropogenic emissions of reactive gases and aerosols from the Community Emissions Data System (CEDS), Geosci. Model Dev., 11, 369–408, https://doi.org/10.5194/gmd-11-369-2018, 2018.

Hurrell, J. W., Holland, M. M., Gent, P. R., Ghan, S., Kay, J. E., Kushner, P. J., Lamarque, J. F., Large, W. G., Lawrence, D., Lind- say, K., Lipscomb, W. H., Long, M. C., Mahowald, N., Marsh, D. R., Neale, R. B., Rasch, P., Vavrus, S., Vertenstein, M., Bader, D., Collins, W. D., Hack, J. J., Kiehl, J., and Marshall, S.: The Community Earth System Model A Framework for Collaborative Research, B. Am. Meteorol. Soc., 94, 1339–1360, https://doi.org/10.1175/BAMS-D-12-00121.1, 2013.

Jonson, J. E., Schulz, M., Emmons, L., Flemming, J., Henze, D., Sudo, K., Tronstad Lund, M., Lin, M., Benedictow, A., Koffi, B., Dentener, F., Keating, T., Kivi, R., and Davila, Y.: The effects of intercontinental emission sources on European air pollution levels, Atmos. Chem. Phys., 18, 13655–13672, https://doi.org/10.5194/acp-18-13655-2018, 2018.

Karamchandani, P., Long, Y., Pirovano, G., Balzarini, A., and Yarwood, G.: Source-sector contributions to European ozone and fine PM in 2010 using AQMEII modeling data, Atmos. Chem. Phys., 17, 5643-5664, https://doi.org/10.5194/acp-17-5643-2017, 2017.

Koo, B., Wilson, G. M., Morris, R. E., Dunker, A. M., and Yarwood, G.: Comparison of source apportionment and sensitivity analysis in a particulate matter air quality model, Environ. Sci. Technol., 43, 6669–6675, https://doi.org/10.1021/es9008129, 2009.

Lelieveld, J., Klingmüller, K., Pozzer, A., Burnett, R. T., Haines, A. and Ramanathan, V.: Effects of fossil fuel and total anthropogenic emission removal on public health and climate, Proc. Natl. Acad. Sci., 116, 7192–7197, https://doi.org/10.1073/pnas.1819989116, 2019.

Li, C., McLinden, C., Fioletov, V., Krotkov, N., Carn, S., Joiner, J., Streets, D., He, H., Ren, X., Li, Z., and Dickerson, R. R.: India Is Overtaking China as the

553   World's Largest Emitter of Anthropogenic Sulfur Dioxide, Scientific Reports, 7,
554   14304, https://doi.org/10.1038/s41598-017-14639-8, 2017.
555

556 O'Neill, B. C., Tebaldi, C., van Vuuren, D. P., Eyring, V., Friedlingstein, P., Hurtt, G.,
557   Knutti, R., Kriegler, E., Lamarque, J.-F., Lowe, J., Meehl, G. A., Moss, R., Riahi,
558   K., and Sanderson, B. M.: The Scenario Model Intercomparison Project
559   (ScenarioMIP) for CMIP6, Geosci. Model Dev., 9, 3461–3482,
560   https://doi.org/10.5194/gmd-9-3461-2016, 2016.
561

562 Persad, G. G., and Caldeira, K.: Divergent global‐scale temperature effects from
563   identical aerosols emitted in different regions, Nat. Commun., 9, 3289.
564   https://doi.org/10.1038/s41467‐018‐05838‐6, 2018.
565

566 Riahi, K., van Vuuren, D. P., Kriegler, E., Edmonds, J., O'Neill, B. C., Fujimori, S.,
567   Bauer, N., Calvin, K., Dellink, R., Fricko, O., Lutz, W., Popp, A., Crespo
568   Cuaresma, J., KC, S., Leimbach, M., Jiang, L., Kram, T., Rao, S., Emmerling, J.,
569   Ebi, K., Hasegawa, T., Havlik, P., Humpenöder, F., Aleluia Da Silva, L., Smith,
570   S., Stehfest, E., Bosetti, V., Eom, J., Gernaat, D., Ma- sui, T., Rogelj, J., Strefler,
571   J., Drouet, L., Krey, V., Luderer, G., Harmsen, M., Takahashi, K., Baumstark, L.,
572   Doelman, J., Kainuma, M., Klimont, Z., Marangoni, G., Lotze-Campen, H.,
573   Obersteiner, M., Tabeau, A., and Tavoni, M.: The Shared Socioeconomic
574   Pathways and their energy, land use, and greenhouse gas emissions
575   implications: An Overview, Global Environ. Chang., 42, 153–168,
576   https://doi.org/10.1016/j.gloenvcha.2016.05.009, 2017.
577

578 Sartelet, K. N., Couvidat, F., Seigneur, C., and Roustan, Y.: Impact of biogenic
579   emissions on air quality over Europe and North America, Atmos. Environ., 53,
580   131–141, https://doi.org/10.1016/j.atmosenv.2011.10.046, 2012.
581

582 Skyllakou, K., Murphy, B. N., Megaritis, A. G., Fountoukis, C., and Pandis, S. N.:
583   Contributions of local and regional sources to fine PM in the megacity of Paris,
584   Atmos. Chem. Phys., 14, 2343– 2352, https://doi.org/10.5194/acp-14-2343-
585   2014, 2014.
586

587 Smith, S. J., van Aardenne, J., Klimont, Z., Andres, R. J., Volke, A., and Delgado
588   Arias, S.: Anthropogenic sulfur dioxide emissions: 1850–2005, Atmos. Chem.
589   Phys., 11, 1101-1116, https://doi.org/10.5194/acp-11-1101-2011, 2011.
590

591 Stjern, C. W., Samset, B. H., Myhre, G., Bian, H., Chin, M., Davila, Y., Dentener, F.,
592   Emmons, L., Flemming, J., Haslerud, A. S., Henze, D., Jonson, J. E., Kucsera,
593   T., Lund, M. T., Schulz, M., Sudo, K., Takemura, T., and Tilmes, S.: Global and
594   regional radiative forcing from 20 % reductions in BC, OC and SO4 – an HTAP2
595   multi-model study, Atmos. Chem. Phys., 16, 13579–13599,
596   https://doi.org/10.5194/acp-16-13579-2016, 2016.

597

598 Stjern, C. W., Stohl, A., and Kristjánsson, J. E.: Have aerosols affected trends in
599   visibility and precipitation in Europe?, J. Geophys. Res., 116, D02212,
600   https://doi.org/10.1029/2010JD014603, 2011.

601

602 Streets, D. G., Tsai, N. Y., Akimoto, H., and Oka, K.: Sulfur dioxide emissions in Asia
603   in the period 1985–1997, Atmos. Environ., 34, 4413–4424,
604   https://doi.org/10.1016/S1352-2310(00)00187-4, 2000.

605

606 Tagaris, E., Sotiropoulou, R., Gounaris, N., Andronopoulos, S., and Vlachogiannis,
607   D.: Effect of the Standard Nomenclature for Air Pollution (SNAP) categories on
608   air quality over Europe, Atmosphere, 6, 1119, doi:10.3390/atmos6081119, 2015.

609

610 Tørseth, K., Aas, W., Breivik, K., Fjæraa, A. M., Fiebig, M., Hjellbrekke, A. G., Lund
611   Myhre, C., Solberg, S., and Yttri, K. E.: Introduction to the European Monitoring
612   and Evaluation Programme (EMEP) and observed atmospheric composition
613   change during 1972–2009, Atmos. Chem. Phys., 12, 5447-5481,
614   https://doi.org/10.5194/acp-12-5447-2012, 2012.

615

616 van Marle, M. J. E., Kloster, S., Magi, B. I., Marlon, J. R., Daniau, A.-L., Field, R. D.,
617   Arneth, A., Forrest, M., Hantson, S., Kehrwald, N. M., Knorr, W., Lasslop, G., Li,
618   F., Mangeon, S., Yue, C., Kaiser, J. W., and van der Werf, G. R.: Historic global
619   biomass burning emissions for CMIP6 (BB4CMIP) based on merging satellite
620   observations with proxies and fire models (1750–2015), Geosci. Model Dev., 10,
621   3329–3357, https://doi.org/10.5194/gmd-10-3329-2017, 2017.

622

623 Vautard, R., Yiou, P., and Oldenborgh, G.: Decline of fog, mist and haze in Europe
624   over the past 30 years, Nat. Geosci., 2, 115–119,
625   https://doi.org/10.1038/ngeo414, 2009.

626

627 Wang, H., Easter, R. C., Rasch, P. J., Wang, M., Liu, X., Ghan, S. J., Qian, Y., Yoon,
628   J.-H., Ma, P.-L., and Vinoj, V.: Sensitivity of remote aerosol distributions to
629   representation of cloud–aerosol interactions in a global climate model, Geosci.
630   Model Dev., 6, 765–782, https://doi.org/10.5194/gmd-6-765-2013, 2013.

631

632 Wang, H., Rasch, P. J., Easter, R. C., Singh, B., Zhang, R., Ma, P.-L., Qian, Y.,
633   Ghan, S. J., and Beagley, N.: Using an explicit emission tagging method in
634   global modeling of source-receptor relationships for black carbon in the Arctic:
635   Variations, sources, and transport pathways, J. Geophys. Res.-Atmos., 119,
636   12888–12909, https://doi.org/10.1002/2014JD022297, 2014.

637

638 Wild, M.: Global dimming and brightening: A review, J. Geophys. Res., 114,
639   D00D16, https://doi.org/10.1029/2008JD011470, 2009.

640

641 Yang, Y., Wang, H., Smith, S. J., Ma, P.-L., and Rasch, P. J.: Source attribution of
642   black carbon and its direct radiative forcing in China, Atmos. Chem. Phys., 17,
643   4319-4336, https://doi.org/10.5194/acp-17-4319-2017, 2017a.
644
645 Yang, Y., Wang, H., Smith, S. J., Easter, R., Ma, P.-L., Qian, Y., Yu, H., Li, C., and
646   Rasch, P. J.: Global source attribution of sulfate concentration and direct and
647   indirect radiative forcing, Atmos. Chem. Phys., 17, 8903-8922,
648   https://doi.org/10.5194/acp-17-8903-2017, 2017b.
649
650 Yang, Y., Wang, H., Smith, S. J., Zhang, R., Lou, S., Yu, H., Li, C., and Rasch, P. J.:
651   Source apportionments of aerosols and their direct radiative forcing and long-
652   term trends over continental United States, Earth's Future, 6, 793–808,
653   https://doi.org/10.1029/2018EF000859, 2018a.
654
655 Yang, Y., Wang, H., Smith, S. J., Zhang, R., Lou, S., Qian, Y., Ma, P.-L., and Rasch,
656   P. J.: Recent intensification of winter haze in China linked to foreign emissions
657   and meteorology, Sci. Rep., 8, 2107, https://doi.org/10.1038/s41598-018-20437-
658   7, 2018b.
659
660 Yang, Y., Smith, S. J., Wang, H., Lou, S., and Rasch, P. J.: Impact of anthropogenic
661   emission injection height uncertainty on global sulfur dioxide and aerosol
662   distribution, J. Geophys. Res.-Atmos., 124, 4812–4826.
663   https://doi.org/10.1029/2018JD030001, 2019.
664
665 Zhang, Q., Jiang, X., Tong, D., Davis, S. J., Zhao, H., Geng, G., Feng, T., Zheng, B.,
666   Lu, Z., Streets, D. G., Ni, R., Brauer, M., van Donkelaar, A., Martin, R. V., Huo,
667   H., Liu, Z., Pan, D., Kan, H., Yan, Y., Lin, J., He, K., and Guan, D.:
668   Transboundary health impacts of transported global air pollution and
669   international trade, Nature, 543, 705–709, https://doi.org/10.1038/nature21712,
670   2017.
671
672
673

674 **Table 1.** Annual emissions (Tg yr^{-1}), concentrations (μg m^{-3}), column burden (mg m^{-2})
675), AOD (scaled up by a factor of 100) and DRF (W m^{-2}) of Sulfate, BC, POA, SBP
676 (sulfate-BC-POA) and SBP-SOA (sulfate-BC-POA-SOA) in Europe averaged over
677 1980–1984 and 2014–2018, as well as the differences between 1980–1984 and
678 2014–2018. Differences in percentage relative to mean values in 1980–1984 are
679 presented in parentheses.
680

		Emis.	Conc.	Burden	AOD*100	DRF
Sulfate	1980–1984	15.10	6.00	14.35	9.13	-3.27
	2014–2018	2.53	1.80	5.79	3.24	-1.24
	Δ	-12.57 (-83.2)	-4.20 (-70.0)	-8.55 (-59.6)	-5.89 (-64.6)	2.04 (-62.2)
BC	1980–1984	0.47	0.4	0.38	0.7	--
	2014–2018	0.25	0.23	0.28	0.5	--
	Δ	-0.22 (-45.8)	-0.17 (-43.0)	-0.11 (-27.6)	-0.21 (-29.2)	--
POA	1980–1984	1.24	1.12	1.12	0.63	--
	2014–2018	0.94	0.86	1.08	0.58	--
	Δ	-0.30 (-24.4)	-0.26 (-23.2)	-0.04 (-3.8)	-0.05 (-7.5)	--
Sulfate-BC-POA	1980–1984	--	7.52	15.85	10.46	--
	2014–2018	--	2.89	7.15	4.32	--
	Δ	--	-4.63 (-61.6)	-8.70 (-54.9)	-6.15 (-58.7)	--
SBP-SOA	1980–1984	--	10.48	19.58	11.92	--
	2014–2018	--	4.34	8.55	5.44	--
	Δ	--	-6.14 (-58.6)	-11.03 (-56.3)	-6.48 (-54.37)	--

681
682

683   **Table 2.** Relative contributions (%) of emissions from major source regions to the
684   changes in near-surface concentrations, column burden, AOD and DRF in Europe
685   between 1980–1984 and 2014–2018.
686

	Sulfate-BC-POA			
	Δ Conc.	Δ Burden	Δ AOD	
EUR	92.8	91.2	91.2	
NAM	1.8	10.0	6.5	
NAF	-1.0	-1.5	-1.6	
MDE	-0.9	-1.9	-1.5	
EAS	-0.3	-3.1	-1.7	
RBU	8.0	9.2	8.5	
OTH	-0.1	-4.2	-2.0	
OCN	-0.3	0.2	0.6	
	Sulfate			
	Δ Conc.	Δ Burden	Δ AOD	Δ DRF
EUR	91.3	89.2	88.9	88.2
NAM	2.1	10.5	6.9	
NAF	-0.6	-0.9	-0.8	
MDE	-0.8	-1.7	-1.3	
EAS	-0.3	-2.8	-1.4	11.8
RBU	8.6	9.5	8.7	
OTH	-0.1	-4.0	-1.8	
OCN	-0.3	0.3	0.7	

687
688
689

690

691
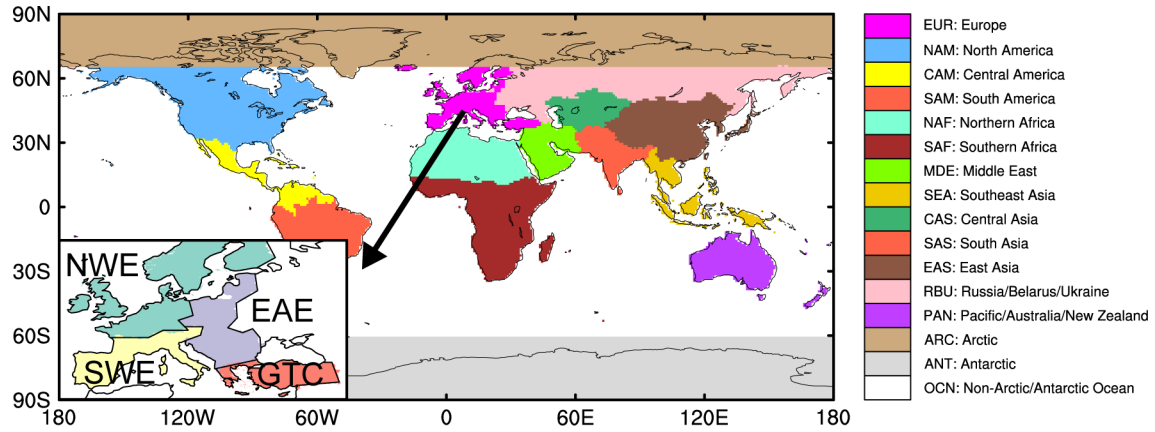
Figure 1. Source regions that are selected for the Explicit Aerosol Source Tagging (EAST) in this study, including Europe (EUR), North America (NAM), Central America (CAM), South America (SAM), North Africa (NAF), South Africa (SAF), the Middle East (MDE), Southeast Asia (SEA), Central Asia (CAS), South Asia (SAS), East Asia (EAS), Russia-Belarus-Ukraine (RBU), Pacific-Australia-New Zealand (PAN), the Arctic (ARC), Antarctic (ANT), and Non-Arctic/Antarctic Ocean (OCN). The embedded panel (at bottom left) is Europe, as the receptor region, which is further divided to Northwestern Europe (NWE), Southwestern Europe (SWE), Eastern Europe (EAE) and Greece-Turkey-Cyprus (GTC).

701

a NMB = -14% R = 0.62
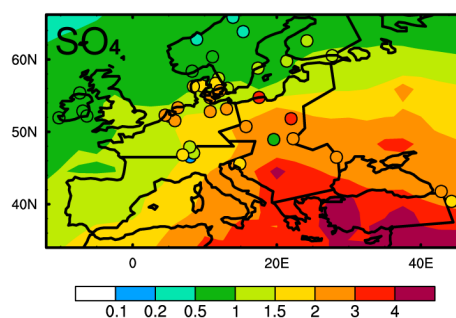
b NMB = -13% R = 0.43
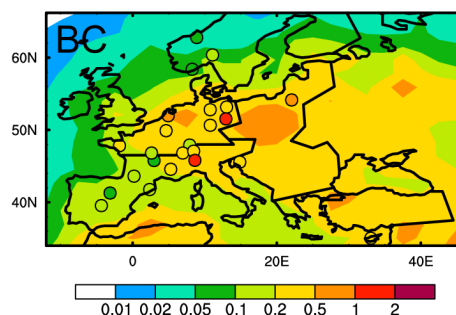
c NMB = -23% R = 0.57
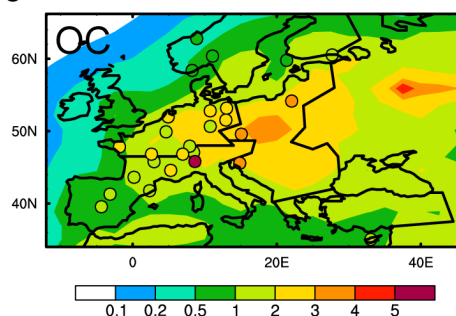
Figure 2. Spatial distribution of simulated (contour) and observed (color-filled circles) annual mean near-surface (a) sulfate, (b) BC, and (c) OC (derived as (POA+SOA)/1.4 in model) concentrations (µg m^{-3}) over 2010–2014. Observations are from EMEP (European Monitoring and Evaluation Programme) networks. Normalized mean bias (NMB = 100%× $\sum (Model_{site} - Observation_{site}) / \sum Observation_{site}$) and correlation coefficient (R) between observed and simulated concentrations are noted at the top of each panel.

712

713
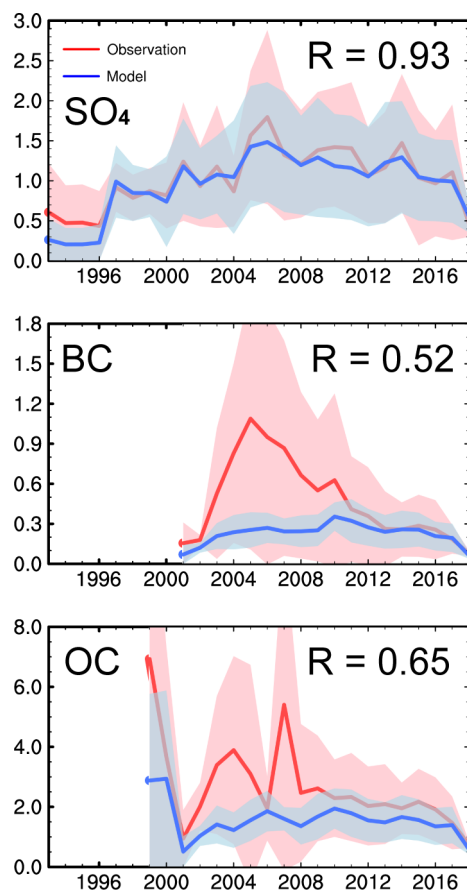
714 **Figure 3.** Time series (1993–2018) of spatial and annual mean near-surface (a)

715 sulfate, (b) BC, and (c) OC concentrations (µg m^{-3}) in Europe from model simulation

716 (blue lines) and observations (red lines). Model results are plotted only when EMEP

717 observational data are available. Shaded areas represent 1-σ spatial standard

718 deviation of annual mean concentrations for each year. Temporal correlation

719 coefficients (R) between observed and simulated spatially averaged concentrations

720 are noted on the top-right corner of each panel.

721

722
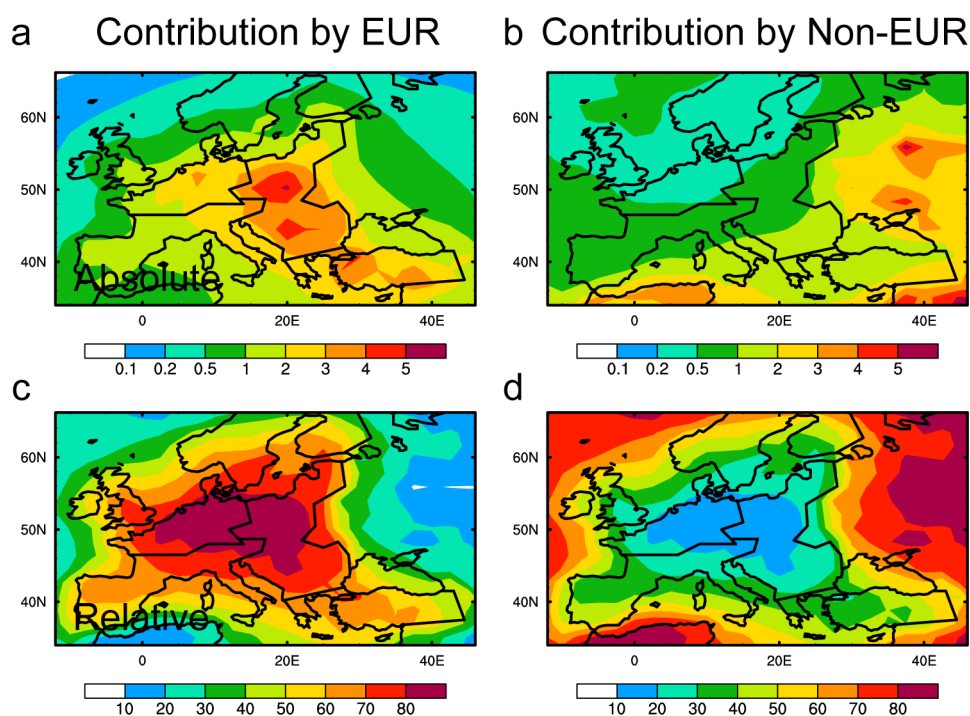
723
724
725 **Figure 4.** (a,b) Absolute (µg m^{-3}) and (c,d) relative contributions (%) to annual mean
726 near-surface concentrations of sulfate-BC-POA from European local emissions
727 (EUR) and emissions outside the Europe (Non-EUR), respectively, averaged over
728 2010–2018.
729
730

731

732
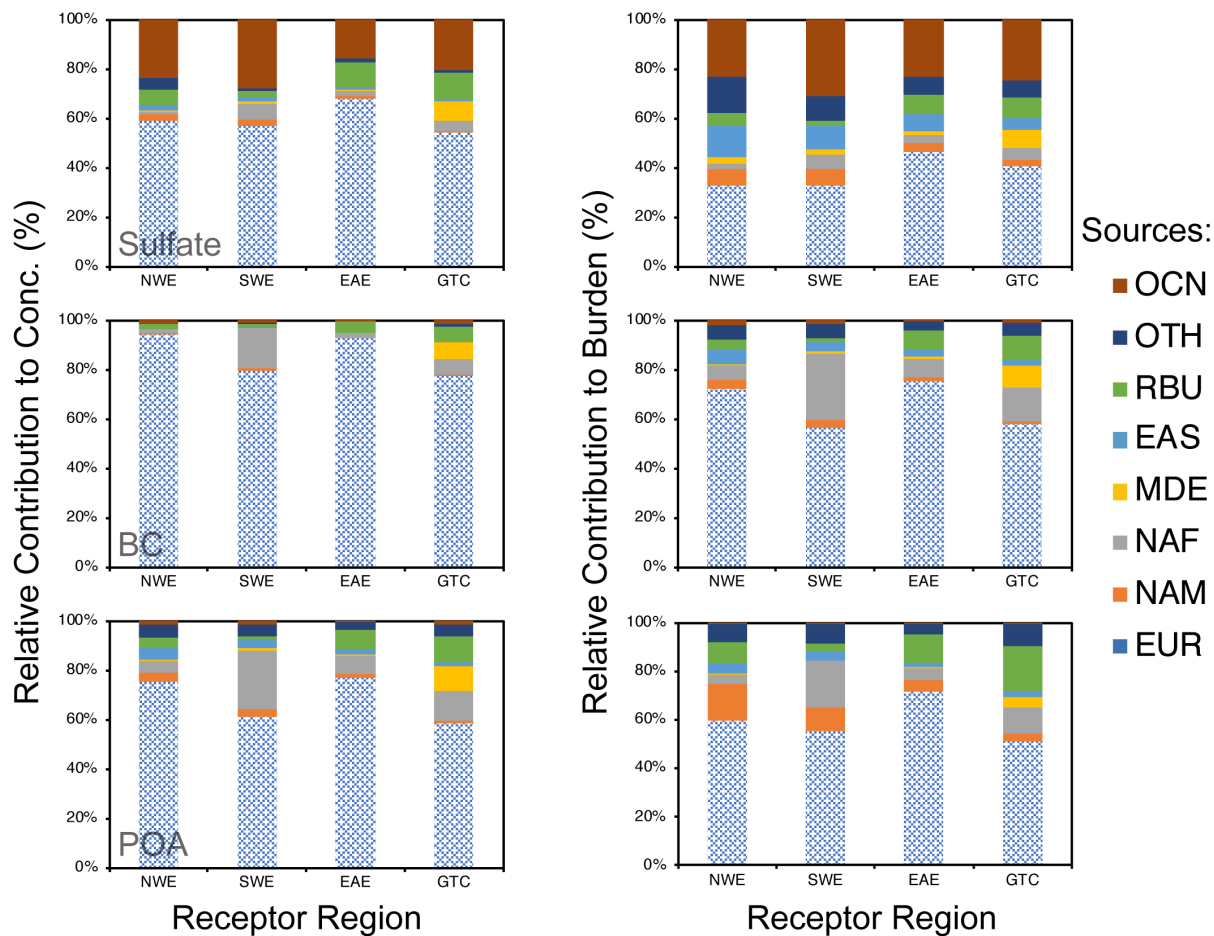
Figure 5. Relative contributions (%) by emissions from major tagged source regions
including Europe (EUR), North America (NAM), North Africa (NAF), the Middle East
(MDE), East Asia (EAS), Russia-Belarus-Ukraine (RBU), Non-Arctic/Antarctic Ocean
(OCN) and other (OTH) regions to near-surface concentrations (left) and column
burdens (right) of sulfate, BC and POA (from top to bottom) in the four sub-regions of
Europe averaged over 2010–2018. Patterned areas represent EUR local
contributions.

740

741
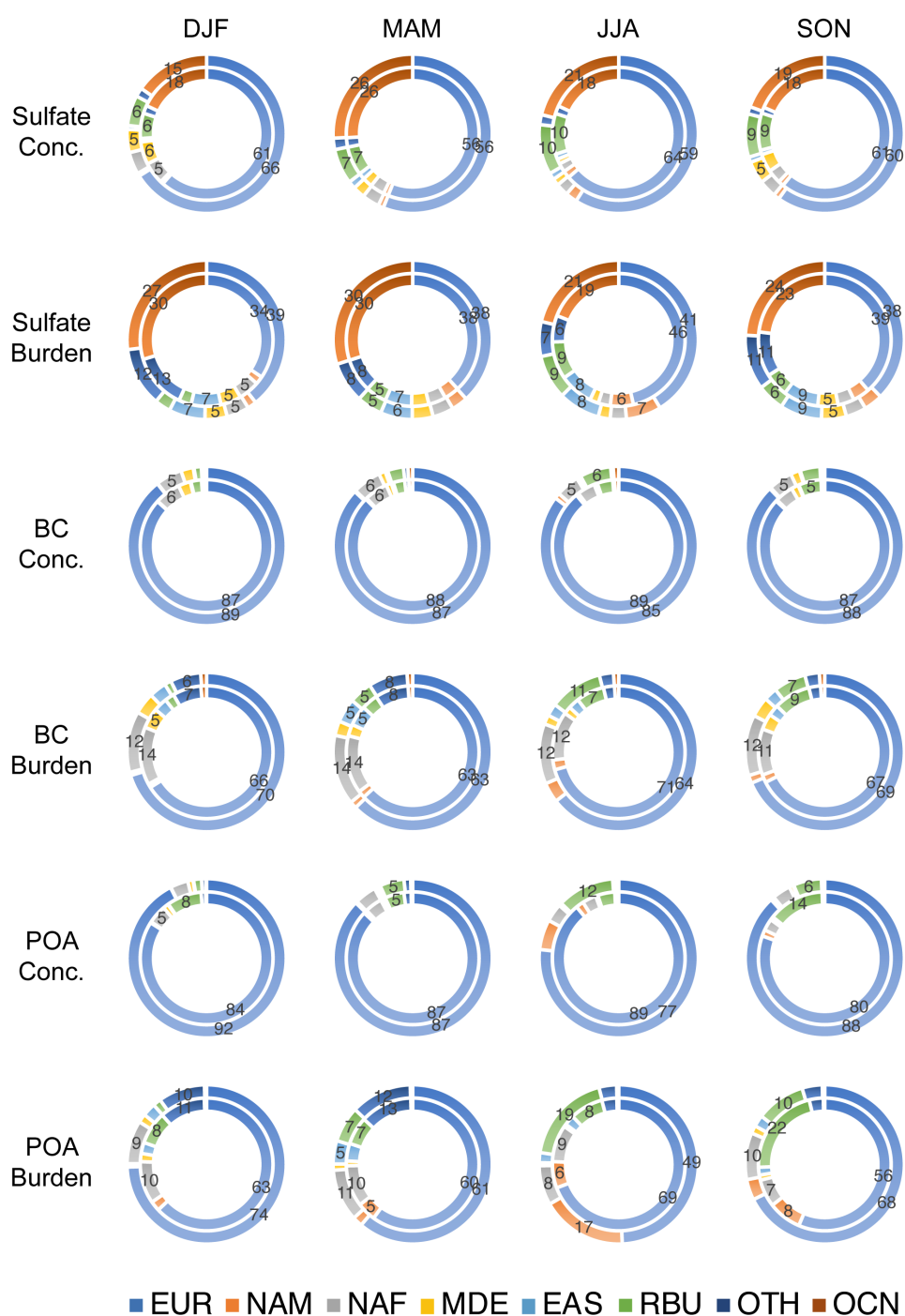
742
743
744 **Figure 6.** Relative contributions (%) by emissions from major tagged source regions
745 to near-surface concentrations (Conc.) and column burdens of December-January-
746 February (DJF), March-April-May (MAM), June-July-August (JJA) and September-
747 October-November (SON) mean sulfate, BC and POA over the Europe averaged
748 over 2010–2018. Outer rings represent the modeled values and the relative
749 contributions in inner rings is calculated based on absolute values normalized by the
750 ratio of seasonal emission to annual mean. Values larger than 5% are marked.
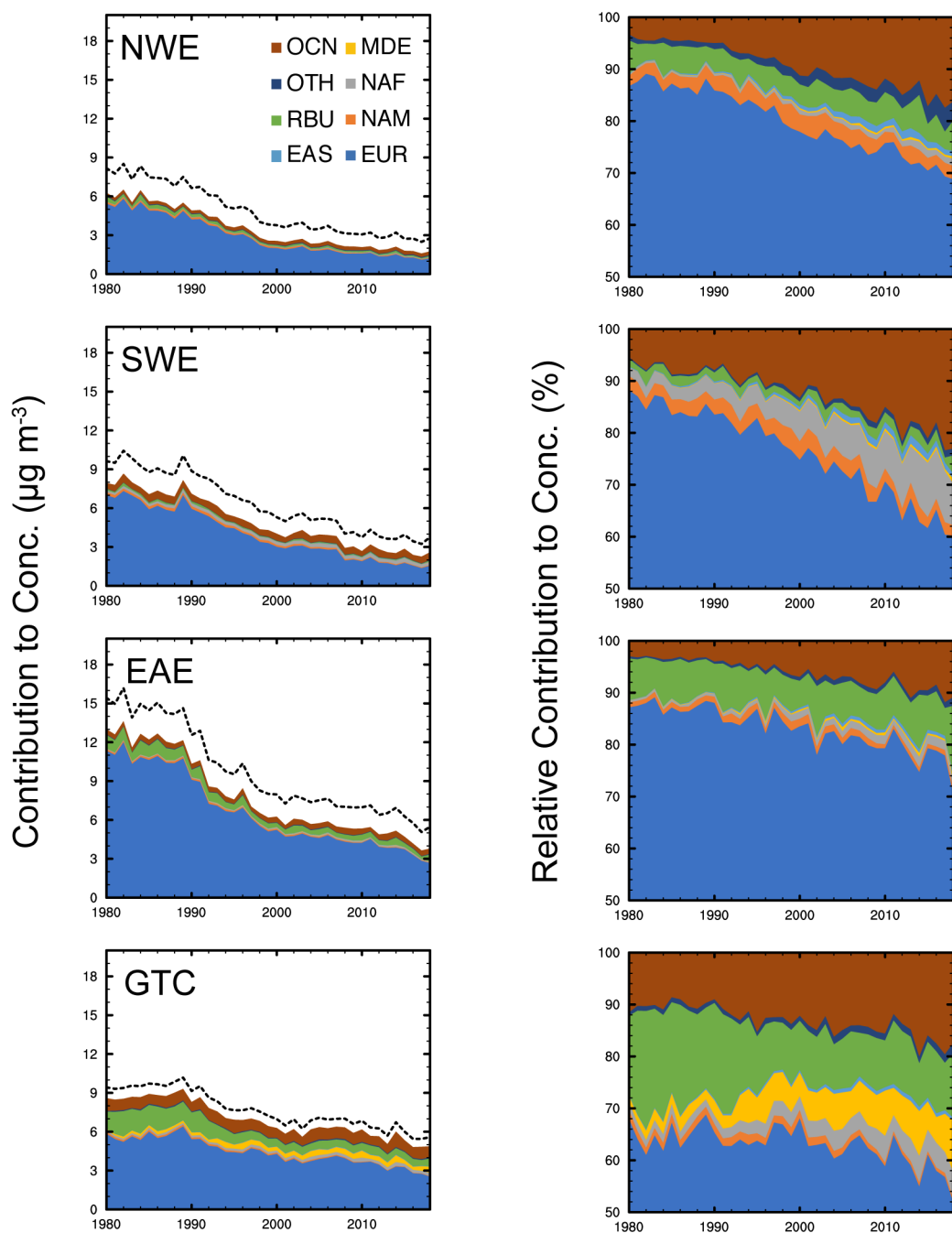
Figure 7. Time series (1980–2018) of absolute (left, µg m⁻³) and relative (right, %) contributions of emissions from major source regions to the simulated annual mean near-surface sulfate-BC-POA concentrations averaged over the four sub-regions of Europe. Dashed lines in left panels represent simulated aerosol concentrations including SOA.
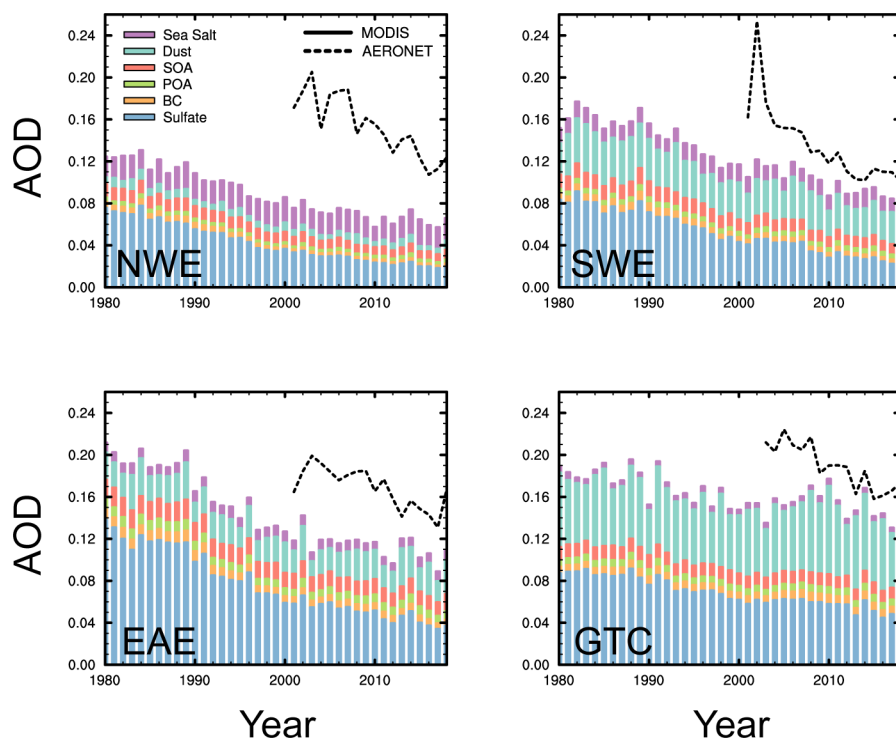
Figure 8. Time series (1980–2018) of simulated annual mean AOD for sulfate, BC, POA, SOA, dust and sea salt averaged over the four sub-regions of Europe. Dashed lines represent AOD from AERONET measurements.

767

768
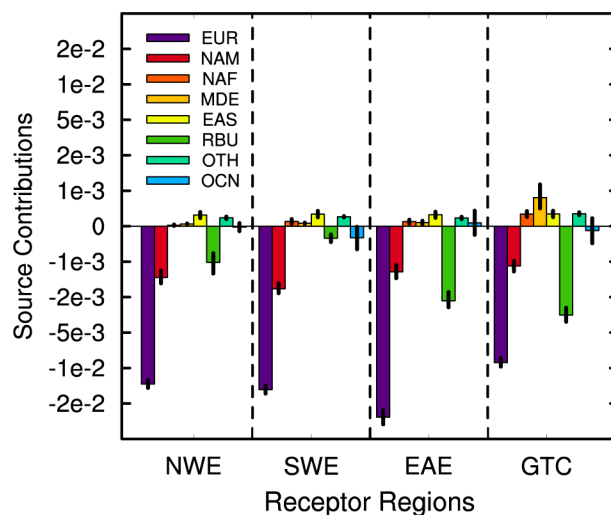
769 **Figure 9.** Absolute contributions (decade^{-1}) of the emissions from major source
770 regions to the trends of sulfate AOD over the four sub-regions of Europe. Error bars
771 represent 95% confidence intervals of the linear regression.

772

773
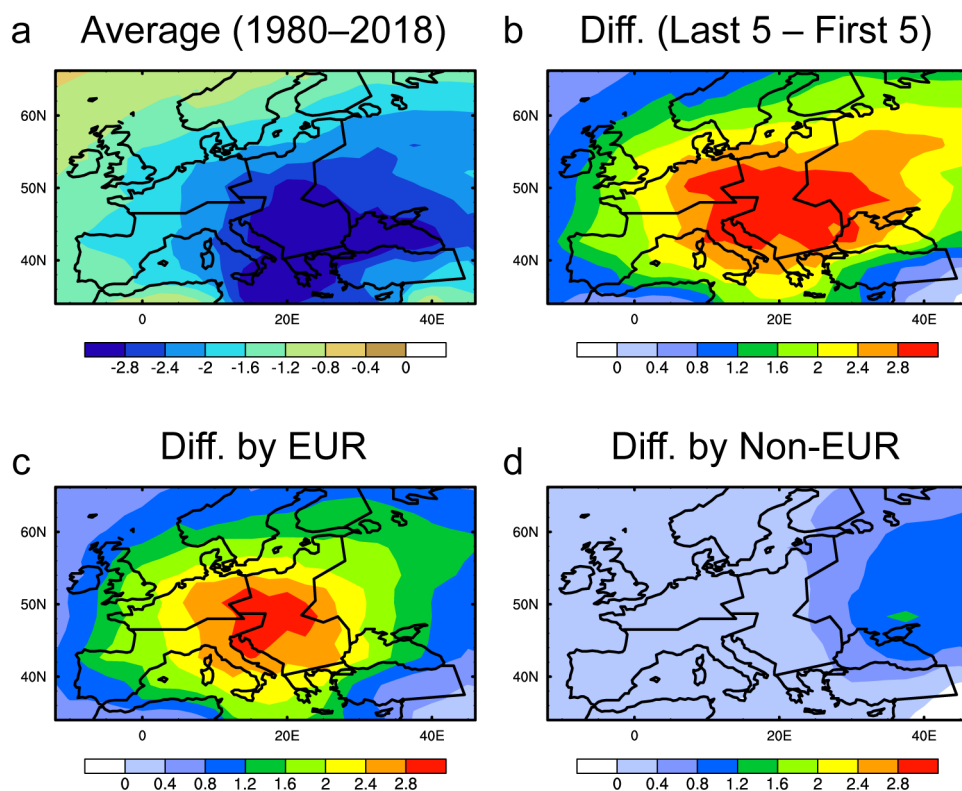
774
775
776 **Figure 10.** (a) Simulated annual mean DRF (W m⁻²) of sulfate averaged over 1980–
777 2018 and (b) the difference in sulfate DRF between 1980–1984 and 2014–2018. The
778 contributions of European and non-European emissions to the difference are given in
779 (c) and (d), respectively.
780

781

782
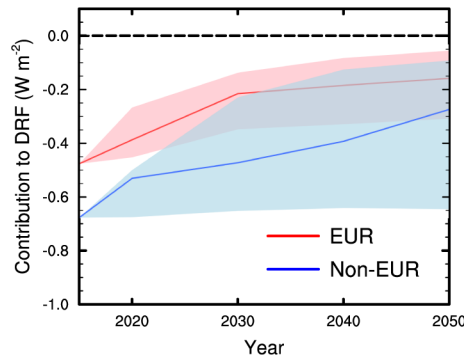
783 **Figure 11.** Time series (2015–2050) of estimated annual mean sulfate DRF over
784 Europe contributed by European and non-European emissions. Lines and areas
785 represent median values and minimum-to-maximum ranges of the estimated sulfate
786 DRF from eight SSP scenarios, including SSP1-1.9, SSP1-2.6, SSP2-4.5, SSP3-7.0,
787 SSP4-3.4, SSP4-6.0, SSP5-3.4, and SSP5-8.5. Future DRF of sulfate aerosol over
788 Europe is estimated by scaling historical mean (1980–2018) sulfate DRF using the
789 ratio of SSPs future SO_2 emissions to historical emissions assuming a linear
790 response of DRF to regional emissions.

791